

This discussion paper is/has been under review for the journal SOIL. Please refer to the corresponding final paper in SOIL if available.

# Assessing the performance of a plastic optical fiber turbidity sensor for measuring post-fire erosion from plot to catchment scale

J. J. Keizer<sup>1</sup>, M. A. S. Martins<sup>1</sup>, S. A. Prats<sup>1</sup>, L. F. Santos<sup>1</sup>, R. Nogueira<sup>2</sup>, and L. Bilro<sup>2</sup>

<sup>1</sup>Earth surface processes team, Centre for Environmental and Marine Studies (CESAM), Dept. Environment and Planning, University of Aveiro, Campus Universitário de Santiago, 3810-193 Aveiro, Portugal

<sup>2</sup>Institute for Telecommunications, Aveiro (IT-Aveiro), Campus Universitário de Santiago, 3810-193 Aveiro, Portugal

Received: 13 April 2015 – Accepted: 7 May 2015 – Published: 11 May 2015

Correspondence to: J. J. Keizer (jjkeizer@ua.pt)

Published by Copernicus Publications on behalf of the European Geosciences Union.

SOILD

2, 449–475, 2015

Testing the performance of a turbidity sensor for post-fire runoff

J. J. Keizer et al.

Discussion Paper	<a href="#">Title Page</a>
	<a href="#">Abstract</a> <a href="#">Introduction</a>
	<a href="#">Conclusions</a> <a href="#">References</a>
	<a href="#">Tables</a> <a href="#">Figures</a>
	<a href="#">◀</a> <a href="#">▶</a>
	<a href="#">◀</a> <a href="#">▶</a>
	<a href="#">Back</a> <a href="#">Close</a>
	<a href="#">Full Screen / Esc</a>
Discussion Paper	<a href="#">Printer-friendly Version</a>
	<a href="#">Interactive Discussion</a>

## Abstract

This study is the first comprehensive testing of a novel plastic optical fiber turbidity sensor with runoff samples collected in the field and, more specifically, with a total of 158 streamflow samples and 925 overland flow samples from a recently burnt forest area in north-central Portugal, collected mainly during the first year after the wildfire, as well as with 56 overland flow samples from a nearby long-unburnt study site. Sediment concentrations differed less between overland flow and streamflow samples than between study sites and, at one study site, between plots with and without effective erosion mitigation treatments. Maximum concentrations ranged from 0.91 to 8.19 g L<sup>-1</sup> for the micro-plot overland flow samples from the six burnt sites, from 1.74 to 8.99 g L<sup>-1</sup> for the slope-scale overland flow samples from these same sites, and amounted to 4.55 g L<sup>-1</sup> for the streamflow samples. Power functions provided (reasonably) good fits to the – expected – relationships of increasing normalized light loss with increasing sediment concentrations for the different sample types from individual study sites. The corresponding adjusted  $R^2$ 's ranged from 0.64 to 0.81 in the case of the micro-plot samples from the six burnt sites, from 0.72 to 0.89 in the case of the slope-scale samples from these same sites, and was 0.85 in the case of the streamflow samples. While the overall performance of the sensor was thus rather satisfactory, the results pointed to the need for scale- and/or site-specific calibrations to maximize reliability of the predictions of sediment concentration by the POF sensor. This especially applied to the cases in which sediment concentration were comparatively low, for example following mulching with forest residues.

## 1 Introduction

Wildfires are now widely recognized as a potential driver of conspicuous changes in geo-morphological and hydrological processes, through their direct effects on vegetation, litter layer and topsoil (Shakesby, 2011; Moody et al., 2013). Studies across the

Title Page

Abstract

Introduction

Conclusions

References

Tables

Figures

◀

▶

◀

▶

Back

Close

Full Screen / Esc

Printer-friendly Version

Interactive Discussion



## Testing the performance of a turbidity sensor for post-fire runoff

J. J. Keizer et al.

[Title Page](#)

[Abstract](#)

[Introduction](#)

[Conclusions](#)

[References](#)

[Tables](#)

[Figures](#)

[◀](#)

[▶](#)

[◀](#)

[▶](#)

[Back](#)

[Close](#)

[Full Screen / Esc](#)

[Printer-friendly Version](#)

[Interactive Discussion](#)



globe have shown strong and sometimes extreme responses in runoff and erosion in recently burnt areas, especially during the earlier stages of the so-called window-of-disturbance (e.g. Cerdà, 1998; Lane et al., 2006; Robichaud et al., 2007). Nonetheless, there remain important research gaps with respect to wildfire impacts on runoff and especially soil erosion, in part due to the relatively limited number of post-fire erosion studies as compared to erosion studies in agricultural areas (Shakesby, 2011). The latter is well-illustrated by the four studies that appear to have been carried out in the Mediterranean Basin on sediment yields from recently burnt catchments (Lavabre and Martin, 1997; Inbar et al., 1998; Mayor et al., 2007; Keizer et al., 2015). Clearly more studies have been published on post-fire erosion at the plot-to-slope scale in the Mediterranean Basin (e.g. Thomas et al., 1999; Fernández et al., 2007; Prats et al., 2014). However, they have typically addressed soil losses with a relatively coarse temporal resolution, i.e. multiple runoff events, which is hampering further insight in underlying sediment transport processes.

The advantages of employing turbidity sensors in erosion studies has been increasingly recognized since their introduction more than two decades ago (Downing, 2006). Nonetheless, commercially-available turbidity sensors such as the “OBS-3+ Suspended Solids and Turbidity Monitor” (© Campbell) typically require complex installations, extensive calibration to local conditions, and, perhaps most importantly, considerable financial resources for their purchase. Fiber optical turbidity sensors and, in particular, those using plastic optical fibers (POF) are now widely viewed to offer various important advantages over traditional methods of sensing (Zienmann, 2008). POF sensors are not only comparatively inexpensive but also easy to handle, immune to electromagnetic interferences, and can easily be used in multi-sensor schemes (Yeo, 2008). This would, amongst others, allow to obtain continuous in-situ recording of sediment concentrations in plot-scale studies and to reduce substantially laboratory efforts by substituting standard methods for at least a large part of the runoff samples.

Various authors (Ruhl et al., 2001; Campbell et al., 2005; Postolache et al., 2007) have obtained promising results with POF sensors to measure turbidity of aqueous

solutions over the past decade. Nonetheless, in their review study, Omar and Mat-Jafri (2009) identified the need for more extensive testing, in particular also with respect to dependence on particle size. Therefore, this study aimed to further test the performance of the POF sensor developed by Bilro et al. (2010), which had provided promising results for contrasting suspended materials, including ashes from recently burnt areas (Bilro et al., 2011). More specifically, this study wanted to: (i) assess the performance of this sensor for measuring sediment concentration of post-fire runoff generated during the initial stages of the “window-of-disturbance”, when erosion rates are expectedly highest; (ii) evaluate if sensor performance differed for stream flow and for overland flow from erosion plots with contrasting runoff areas (micro-plots vs. slope-scale plots) and, thus, potentially different erosion processes (inter-rill erosion vs. rill/gully erosion); (iii) determine if sensor performance depended on land cover, parent material and site-specific conditions. This study was envisaged as an important step towards the development of a commercial version of the sensor designed by Bilro et al. (2010).

## 2 Study area and sites

This study was carried out near the hamlet of Ermida in the Sever do Vouga municipality of north-central Portugal (Fig. 1). The area was burnt by a wildfire that took place between the 26 and 28 July 2010 and that affected some 300 ha (DUDF, 2011). By the time of the fire, the area was mainly covered by plantations of eucalypt (*Eucalyptus globulus* Labill.) but did include some plantations of maritime pine (*Pinus pinaster* Ait.). The severity of the wildfire (sensu Keely, 2009) was assessed in the field using as indicators ash colour as well as degree of tree crown scorching and of litter layer consumption, following Shakesby and Doerr (2006) and prior studies in the region such as Malvar et al. (2011, 2013). At all six study sites, fire severity was classified as moderate. During the winter of 2010/2011, the central part of the study area was bench terraced using a bull dozer (the terraces are clearly visible in Fig. 1).

<a href="#">Title Page</a>	
<a href="#">Abstract</a>	<a href="#">Introduction</a>
<a href="#">Conclusions</a>	<a href="#">References</a>
<a href="#">Tables</a>	<a href="#">Figures</a>
<a href="#">◀</a>	<a href="#">▶</a>
<a href="#">◀</a>	<a href="#">▶</a>
<a href="#">Back</a>	<a href="#">Close</a>
<a href="#">Full Screen / Esc</a>	
<a href="#">Printer-friendly Version</a>	
<a href="#">Interactive Discussion</a>	



## Testing the performance of a turbidity sensor for post-fire runoff

J. J. Keizer et al.

Title Page

Abstract

Introduction

Conclusions

References

Tables

Figures

◀

▶

◀  
Back

▶  
Close

Full Screen / Esc

Printer-friendly Version

Interactive Discussion



The climate of the study area can be classified as humid meso-thermal (Csb, according to the Köppen classification), with moderately dry but extended summers (DRA-Centro, 1998). The parent material in the study area mainly consisted of pre-Ordovician schists but included Hercynian granites at some locations, as is typical for the Hesperic

5 Massif (Ferreira, 1978). The soils were mapped, at a scale of 1 : 1 000 000, as predominantly Humic Cambisols (Cardoso et al., 1971, 1973). However, field descriptions of soil profiles at the various study sites suggested a prevalence of Leptosols (WRB, 2006) (see Machado et al., 2015; Martins et al., 2013). Soil texture of the A-horizon was also determined in the field, and was slightly coarser for the soils on granite (sandy loam) 10 than for the soils on schist (sandy clay loam). The topsoil was very rich in organic matter, amounting to 20–30 % at 0–2 cm depth (Machado et al., 2015) and 8–11 % at 0–5 cm depth (Prats et al., 2014).

Within the burnt area, a total of six study sites were selected to study post-fire runoff and erosion (Fig. 1). They consisted of four eucalypt plantations on schist, one eucalypt 15 plantation on granite and one pine plantation on schist, basically following the incidence of these land cover-parent material combinations in the burnt area. In addition, a long-unburnt eucalypt plantation was selected in the immediate vicinity of the burnt area. Furthermore, one of the catchments within the burnt area was selected to study the hydrological and erosion response at the catchment scale.

## 20 3 Materials and methods

### 3.1 Collection of runoff samples

The study sites within the burnt area were instrumented with bounded micro-plots (0.25–0.30 m<sup>2</sup>) as well as (un-)bounded slope-scale plots (width of ca. 2 m and area > 50 m<sup>2</sup>), whereas the long-unburnt eucalypt plantation was only instrumented with an 25 unbounded slope-scale plot. The number of micro-plots per site varied between three and four, except in the case of site S where four pairs of three micro-plots were used to

assess the effectiveness of two treatments to reduce soil erosion, i.e. mulching with forest residues and application of a dry granular anionic polyacrylamide (PAM; see Prats et al., 2014). Polyacrylamides has been found to markedly reduce soil losses from agricultural fields and road embankments (Ben-Hur, 2006). Only one slope-scale plot was 5 installed at each site, except in the case of site S where two plots were used to assess the effectiveness of mulching with forest residues to reduce soil erosion. Each slope-scale plot, however, consisted of four sub-plots where runoff was collected. Runoff was collected in tanks of 30–500 L connected to the outlets of the micro-plots or the sub-plots of the slope-scale plots. Runoff was measured and runoff samples were collected 10 at 1- to 2-weekly intervals, depending on rainfall, starting at the end of August 2010 when the site instrumentation had been completed. More details on the experimental set-ups at the different sites as well as on field data and sample collection were given by Machado et al. (2015), Martins et al. (2013) and Prats et al. (2014, 2015).

The outlet of the experimental catchment was instrumented with a hydrological station comprising two flumes, two water level recorders and an automatic sampler that 15 was triggered by a data logger based on the readings of the two water level recorders.

### 3.2 Laboratory analysis of runoff samples

For this study, a total of 1139 runoff samples were analyzed, of which 158 concerned 20 streamflow, and 565 and 416 overland flow at the slope and micro-plot scale, respectively. The samples were all collected during the first year after the wildfire, except for 36 micro-plot samples that were collected at the S site between the end of October 2011 and early January 2012.

The sediment concentration of these samples was determined in the laboratory using 25 the classic filtration method (APHA, 1998), employing paper filters with a pore diameter of 12–14 µm and drying the filters in an oven at 105 °C for 24 h. Furthermore, the organic matter content of the filtered sediments was determined using the loss-on-ignition method, placing the filters in a muffle for 4 h at 550 °C.

[Title Page](#)

[Abstract](#)

[Introduction](#)

[Conclusions](#)

[References](#)

[Tables](#)

[Figures](#)

◀

▶

◀  
Back

▶  
Close

[Full Screen / Esc](#)

[Printer-friendly Version](#)

[Interactive Discussion](#)

For each of the runoff samples, the normalized loss of the transmitted light was determined using the plastic optical fiber (POF) turbidity sensor presented by Bilo et al. (2010) but with a slightly modified design of the sensor head. To this end, the sensor head was first placed within a plastic recipient with bi-distilled water to measure the reference signal and then within a second recipient with the runoff sample to measure the light loss due to the sediments that were being kept in suspension by means of a magnetic agitator. The measurements were carried out during a period of 1 min, during which the POF sensor performed 120 readings. Following visual inspection for and possible elimination of anomalous readings, the average values of both sets of 10 readings were then used to compute the normalized transmitted light loss.

### 3.3 Data analysis

The relationships of sediment concentrations with normalized light loss were determined using the Origin software (© OriginLab). In a first phase, a range of possible functions (first to fourth order polynomials, exponential, Napierian logarithmic and power) were fitted to the entire sets of micro-plot samples, slope-scale samples and catchment-scale samples. Overall, the third and fourth order polynomials and the exponential functions provided the best fits, with identical adjusted  $R^2$ 's (0.73, 0.87 and 0.85, respectively). Nonetheless, the power function was preferred for the ensuing results, since the differences in  $R^2$ 's were considered too small ( $\leq 0.02$ ) to justify the 20 additional one or two unknowns of the other functions.

[Title Page](#)[Abstract](#)[Introduction](#)[Conclusions](#)[References](#)[Tables](#)[Figures](#)[◀](#)[▶](#)[◀](#)[▶](#)[Back](#)[Close](#)[Full Screen / Esc](#)[Printer-friendly Version](#)[Interactive Discussion](#)

## 4 Results and discussion

### 4.1 Micro-plot scale

#### 4.1.1 Within-site differences related to erosion mitigation treatments

In line with the findings of Prats et al. (2014) regarding specific soil losses, the sample sets of the three treatments differed markedly in sediment concentrations (Table 1). For example, the median sediment concentration of the untreated samples was 35 % lower than that of the PAM samples but almost three times higher than that of the mulching samples. The median organic matter contents of the three sample sets (52–67 %) indicated that charred material was a major component of the sediments exported under all three treatments, as was also found by Malvar et al. (2011, 2013) for sediments eroded during the first two years following fire. The median organic matter contents closely matched the average values in Prats et al. (2014), attesting to the representativeness of the sample sets included in this study.

All three sample sets revealed a relationship of increasing normalized light loss with increasing sediment concentration (Fig. 2), as was expected based on the findings with an earlier proto-type of the turbidity sensor (Bilro et al., 2010, 2011). The power function provided reasonably good fits of these relationships in all three instances, with adjusted  $R^2$ 's ranging from 0.64 in the case of the untreated samples to 0.72 in the case of the PAM samples (Table 1). Bilro et al. (2011) found clearly better fits ( $R^2 > 0.95$ ) for clay as well as ash particles but the authors used dilution series of artificial samples rather than runoff samples collected in the field.

The curves fitted to the untreated and the PAM samples were very similar, at least within the range of measured sediment concentrations (i.e.  $< 8.5 \text{ g L}^{-1}$ ). Possibly, the somewhat divergent curve of the mulching samples was due to smaller range of measured sediment concentrations ( $< 2.5 \text{ g L}^{-1}$ ), also because the relationships between sediment concentration and normalized light loss seemed to reveal more spread at higher concentrations.

Testing the performance of a turbidity sensor for post-fire runoff

J. J. Keizer et al.

Title Page

Abstract

Introduction

Conclusions

References

Tables

Figures

◀

▶

◀

▶

Back

Close

Full Screen / Esc

Printer-friendly Version

Interactive Discussion



## 4.1.2 Between-site differences related to land cover and parent material

The six study sites revealed conspicuous differences in the sediment concentrations of the overland flow samples from the – untreated – micro-plots, with, for example, maximum concentrations varying almost an order of a magnitude (0.91 vs. 8.19 g L<sup>-1</sup>;

5 Table 1). Median sediment concentrations appeared to be influenced by both parent material and forest type, as median values were clearly lower for the pine plantation on schist (0.08 g L<sup>-1</sup>) and for the eucalypt plantation on granite (0.13 g L<sup>-1</sup>) than for the eucalypt plantations on schist ( $\geq 0.21$  g L<sup>-1</sup>). At the same time, however, differences were even larger among the four eucalypt plantations on schist, since the median sediment 10 concentration of the D site (0.21 g L<sup>-1</sup>) was around twice as low as that of the B and S sites (0.38–0.41 g L<sup>-1</sup>), and even 3.5 times lower than that of the E site (0.73 g L<sup>-1</sup>). The difference in median sediment concentration between the pine plantation and the eucalypt plantation on granite agreed well with the difference in the sites' median specific sediment losses reported by Martins et al. (2013; 0.08 vs. 0.16 g m<sup>-2</sup> mm<sup>-1</sup> of 15 runoff), once again testifying to the representativeness of the sample sets included in this study. Also, Machado et al. (2015) reported clearly higher average sediment losses at the B site than at the pine plantation as well as the eucalypt plantation on granite (200 vs. 85 vs. 50 g m<sup>-2</sup>).

20 The sample sets from all six study sites showed the expected increases in normalized light loss with increasing sediment concentrations. Furthermore, these increases agreed well with power functions, with the adjusted  $R^2$ 's of the fitted curves ranging from 0.64 to 0.81 (Fig. 3; Table 1). The fits were somewhat worse for sites D and S than for the remaining four sites (adjusted  $R^2$ 's: 0.64–0.67 vs. 0.76–0.81) but this difference was apparently unrelated to parent material, forest type, sediment concentrations or their organic matter contents. However, the shape of the fitted curves did 25 seem related to sediment concentrations. The curves were steeper for sites A, C and D than for sites B, E and S, and the former three sites had clearly lower median, third quartile and maximum sediment concentrations than the latter three sites (e.g., in the

Title Page

Abstract

Introduction

Conclusions

References

Tables

Figures

◀

▶

Back

Close

Full Screen / Esc

Printer-friendly Version

Interactive Discussion



case of maximum concentrations, 0.91–1.48 vs. 3.89–7.48 g L<sup>−1</sup>). This contrast could be due to differences in the size of the exported sediment particles, since the sensor's light attenuation was shown to decrease with increasing particle size (Bilro et al., 2011) and since the lower sediment concentrations at sites A, C and D could be explained by overland flow with a lower transport capacity, preferentially exporting smaller particles. Nonetheless, the contrast could also be an artifact from the lower ranges of sediment concentrations measured at sites A, C and D, as these ranges only covered the initial, steeper parts of the fitted curves.

## 4.2 Slope scale

### 10 4.2.1 Within-site differences related to erosion mitigation treatment

Like the micro-plot samples, the slope-scale samples revealed clear differences in sediment concentrations between the untreated and mulching samples (Table 2). The median sediment concentrations, for example, were more than three times higher in the case of the untreated samples than in the case of the mulching samples, similar to what was found for the micro-plot samples. These differences in sediment concentrations were in line with the fact that the untreated plot produced about twice as much overland flow than the mulched plot during the first year after fire (Prats et al., 2015; 58 vs. 30 mm).

20 The slope-scale samples tended to have higher median, third quartile and maximum sediment concentrations than the micro-plot samples of the same treatment (Table 2). The only exception was the maximum sediment concentration of the mulched samples, being 20 % lower in the case of the slope-scale samples than of the micro-plot samples (1.74 vs. 2.19 g L<sup>−1</sup>). This tendency in sediment concentrations was opposed to that in overland flow, as Prats et al. (2015) reported roughly 15 times less overland flow at the 25 slope than micro-plot scale (409–956 vs. 30–58). The two spatial scales also differed markedly in the median organic matter concentration of the mulching samples, which was 30 % lower in the case of the slope-scale samples (47 vs. 67 %).

<a href="#">Title Page</a>	
<a href="#">Abstract</a>	<a href="#">Introduction</a>
<a href="#">Conclusions</a>	<a href="#">References</a>
<a href="#">Tables</a>	<a href="#">Figures</a>
<a href="#">◀</a>	<a href="#">▶</a>
<a href="#">◀</a>	<a href="#">▶</a>
<a href="#">Back</a>	<a href="#">Close</a>
<a href="#">Full Screen / Esc</a>	
<a href="#">Printer-friendly Version</a>	
<a href="#">Interactive Discussion</a>	

## Testing the performance of a turbidity sensor for post-fire runoff

J. J. Keizer et al.

[Title Page](#)

[Abstract](#)

[Introduction](#)

[Conclusions](#)

[References](#)

[Tables](#)

[Figures](#)

[◀](#)

[▶](#)

[◀](#)

[▶](#)

[Back](#)

[Close](#)

[Full Screen / Esc](#)

[Printer-friendly Version](#)

[Interactive Discussion](#)



The fit of the power function was substantially better for the slope-scale samples than for the micro-plot samples in the case of the untreated plot but basically the same in the case of the mulched plot (Table 2; adjusted  $R^2$ 's: 0.85 vs. 0.64 and 0.71 vs. 0.69, respectively). In both cases, light loss with increasing sediment concentration was larger for the slope-scale samples than for the micro-plot samples (Fig. 4). Only in the case of the mulching samples, however, this was due to a clearly higher attenuation coefficient (0.75 vs. 0.66) and, as referred earlier, could be explained by a greater prevalence of smaller particles in the slope-scale than micro-plot samples (see Bilro et al., 2011), reflecting a reduced transport capacity of the overland flow. This explanation could also account for the lower median organic matter concentration of the slope-scale samples, with the larger charred particles being beyond the runoff's detachment/transport capacity.

### 4.2.2 Between-site differences related to fire, land cover and parent material

The slope-scale samples revealed a strong tendency for higher median, third quartile and maximum sediment concentrations than the micro-plot samples, as was also noted in the previous section. At the same time, however, they suggested similar distinctions between the six burnt study sites, except in the case of the eucalypt plantation on granite (Table 2). The median sediment concentration was 2.5 times lower for the pine plantation on schist ( $0.11 \text{ g L}^{-1}$ ) than for the burnt eucalypt plantations on schist ( $\geq 0.29 \text{ g L}^{-1}$ ), while, among the latter, it was two to four times lower for the D site ( $0.29 \text{ g L}^{-1}$ ) than for the B and S sites ( $0.63 \text{ g L}^{-1}$ ), and for the E site ( $1.28 \text{ g L}^{-1}$ ), respectively. The median sediment concentration for the eucalypt plantation on granite lied within the range of values for the other eucalypt plantations, unlike was the case for the micro-plot samples as a result of a more than five times increase in median concentration from the micro-plot to slope scale. This comparatively large increase in median concentration was in line with the differences in average sediment losses between micro-plot to slope scale reported by Machado et al. (2015) for three of the present study sites: the losses increased noticeably for the eucalypt plantation on granite (from

5 50 to 140 g m<sup>-2</sup>), while they decreased markedly for the pine plantation as well as for the eucalypt plantation on schist at the B site (from 85 and 200 to 3.5 and 6.1 g m<sup>-2</sup>, respectively). The sediment loss figures in Machado et al. (2015) fitted in well with the lower sediment concentrations for the pine plantation than for the eucalypt plantation on schist (site B) but less well with the similar sediment concentrations for the two eucalypt plantations, even though the third quartile value was noticeably higher for the plantation on granite than for that on schist (1.39 vs. 1.09 g L<sup>-1</sup>).

10 The sediment concentrations for the unburnt eucalypt plantation were conspicuously lower than those for any of the burnt eucalypt plantations. For example, the maximum value was less than 1 g L<sup>-1</sup>, and was between 8 and 12 times smaller than those of the burnt eucalypt plantations. This agreed with the slope-scale sediment losses reported by Machado et al. (2015), being clearly lower for the unburnt than burnt eucalypt site on schist (1.2 vs. 3.5 g m<sup>-2</sup>).

15 Better fits of the power function were obtained for the slope-scale samples than for the micro-plot samples in the case of five of the six burnt study sites, the pine site being the exception (Table 2). The pine plantation also stood out for its low adjusted  $R^2$  (0.72) as compared to the other burnt plantations (0.83–0.89). The  $R^2$  was similarly low for the mulching samples (0.71) and even considerably lower for the samples from the unburnt eucalypt stand (0.52), suggesting an association between poor fits and 20 reduced sediment concentrations, unlike was the case for the micro-plot samples.

25 The best-fitting curves for the slope-scale samples revealed a greater similarity between the six burnt plantations than those for the micro-plot samples (Fig. 4). Among the burnt plantations, only the D site stood out but mainly because of a comparatively low base constant rather than a different attenuation coefficient. For the same reason, the curve for the long-unburnt plantation stood out even more from those of the burnt plantations. The discrepancy of these two curves could well be an artifact from the comparatively low sediment concentrations measured at the D and F sites, also because possible differences in particle size due to reduced transport capacity would point to steeper curves as was the case of the curves fitted to the micro-plot samples

Title Page

Abstract

Introduction

Conclusions

References

Tables

Figures

◀

▶

Back

Close

Full Screen / Esc

Printer-friendly Version

Interactive Discussion



of sites A, C and D (see Sect. 4.1.2). Unlike in the case of these latter three sites, the curves fitted to the slope-scale samples of sites B and E agreed particularly well with those fitted to the sites' micro-plot samples. This suggested that wider ranges of measured sediment concentrations provided a more reliable basis for a consistent relation between turbidity and sediment concentrations over spatial scales as well as across study sites.

### 4.3 Catchment scale

The sediment concentrations of the streamflow samples were more similar to those of slope-scale samples from the C site than from the other two sites that were located 10 within the catchment but were less representative of land cover-parent material (Table 3). The third quartile values were especially similar (1.05 and 1.09 g L<sup>-1</sup>), whereas the maximum value of the streamflow samples was well below the maximum values for all three slopes (4.55 vs.  $\geq 6.59$  g L<sup>-1</sup>). Also the median organic matter concentration of the streamflow samples was comparatively low (22 vs.  $\geq 38$  %). Even so, it was 15 substantially higher than the organic matter content of the sediments deposited as bed load within the flume at the catchment outlet (Keizer et al., 2015; 5 %).

The power function provided a good fit to the relationship of increasing normalized light loss with increasing sediment concentration as revealed by the streamflow samples, with an adjusted  $R^2$  of 0.85 (Table 3). The fitted curve, however, differed considerably 20 from the curves fitted to slope-scale samples of the three slopes located within the catchment. The stronger attenuation coefficient for the streamflow samples (0.71 vs. 0.57–0.60) could be due to a prevalence of smaller particles in suspension, especially because of the deposition of sediments in the flume at the catchment outlet as well as in two upstream retention ponds (see Keizer et al., 2015).

<a href="#">Title Page</a>	
<a href="#">Abstract</a>	<a href="#">Introduction</a>
<a href="#">Conclusions</a>	<a href="#">References</a>
<a href="#">Tables</a>	<a href="#">Figures</a>
<a href="#">◀</a> <a href="#">▶</a>	
<a href="#">◀</a>	<a href="#">▶</a>
<a href="#">Back</a>	<a href="#">Close</a>
<a href="#">Full Screen / Esc</a>	
<a href="#">Printer-friendly Version</a>	
<a href="#">Interactive Discussion</a>	

## 5 Conclusions

The principal conclusions of this study into the performance of a novel plastic optical fiber (POF) turbidity sensor for measuring soil erosion following wildfire were the following:

- 5 i. the observed sediment concentrations were within the measurement range of the POF sensor, attesting to the suitability of the sensor to be employed during the initial phases of the so-called window-of-disturbance when erosion losses tend to be highest and when exported sediments tend to contain highest contents of – charred – organic matter;
- 10 ii. the relationships of sediment concentration with normalized light loss varied markedly with spatial scale and, in particular, between micro-plot and slope-scale samples, on the one hand, and, on the other, catchment-scale samples, suggesting that scale-specific calibration curves are required to guarantee optimal sensor performance;
- 15 iii. the slope-scale relationships of sediment concentration with normalized light loss varied clearly less between study sites than the micro-plot scale relationships, indicating that the need for site-specific calibration curves is greater when sediment concentrations and, thus, erosion rates are comparatively low;
- 20 iv. the previous conclusion was also suggested by the comparison of the sediment concentrations with and without an effective erosion mitigation treatment;
- v. the POF sensor would allow to speed up considerably the processing of the runoff samples in the laboratory (and, perhaps, even in the field) and, at the same time, would permit an efficient, stratified-sampling approach towards the construction of scale- and/or site-specific calibration curves.

[Title Page](#)

[Abstract](#)

[Introduction](#)

[Conclusions](#)

[References](#)

[Tables](#)

[Figures](#)

[◀](#)

[▶](#)

[◀](#)

[▶](#)

[Back](#)

[Close](#)

[Full Screen / Esc](#)

[Printer-friendly Version](#)

[Interactive Discussion](#)



*Acknowledgements.* The present study was carried out in the framework of the projects TRANFIBRA (project no. 23148) and FIRECNUTS (PTDC/AGRCFL/104559/2008), funded by FEDER, through the Agência de Inovação S.A., in the framework of the QREN SI I&DT program and funded by FCT/MCTES (PIDAAC), with co-funding by FEDER through COMPETE (Programa Operacional Factores de Competitividade; POFc), respectively. Additional financial support was provided by the EU-FP7 project RECAR (contract number grant agreement 603498).

5 We further gratefully acknowledge the help of various colleagues of the earth surface processes team with field data and sample collection and/or with laboratory analysis of the sediment samples.

## 10 References

APHA (American Public Health Association): Total suspended solids dried at 105 degrees Celsius method 2540D, in: Standard Methods for the Examination of Water and Waste Water, 20th Edn., Washington, DC, USA, 1998.

Ben-Hur, M.: Using synthetic polymers as soil conditioners to control runoff and soil loss in arid regions – a review, *Aust. J. Soil Res.*, 44, 191–204, 2006.

15 Bilver, L., Prats, S. A., Pinto, J. L., Keizer, J. J., and Nogueira, N.: Design and performance assessment of a POF based sensor for measuring water turbidity, *Meas. Sci. Technol.*, 21, 107001, doi:10.1088/0957-0233/21/10/107001, 2010.

20 Bilver, L., Prats, S., Pinto, J. L., Keizer, J. J., and Nogueira, R. N.: Turbidity sensor for determination of concentration, ash presence and particle diameter of sediment suspensions, *Proc. SPIE* 7753, 775356, doi:10.1117/12.885112, 2011.

Campbell, C., Laycak, D., Hoppes, W., Tran, N. T., and Shib, F.: High concentration suspended sediment measurements using a continuous fiber optic in-stream transmissometer, *J. Hydrol.*, 311, 244–253, 2005.

25 Cardoso, J. C., Bessa, M. T., and Marado, M. B.: *Carta dos solos de Portugal (1:1,000,000)*, Serviço de Reconhecimento e de Ordenamento Agrário, Secretaria de Estado da Agricultura, Lisbon, Portugal, 1971.

Cardoso, J. C., Bessa, M. T., and Marado, M. B.: *Carta dos solos de Portugal (1:1,000,000)*, Agronomia Lusitana, 33, 461–602, 1973.

[Title Page](#)

[Abstract](#)

[Introduction](#)

[Conclusions](#)

[References](#)

[Tables](#)

[Figures](#)

◀

▶

[Back](#)

[Close](#)

[Full Screen / Esc](#)

[Printer-friendly Version](#)

[Interactive Discussion](#)



## Testing the performance of a turbidity sensor for post-fire runoff

J. J. Keizer et al.

[Title Page](#)

[Abstract](#)

[Introduction](#)

[Conclusions](#)

[References](#)

[Tables](#)

[Figures](#)

◀

▶

◀

▶

[Back](#)

[Close](#)

[Full Screen / Esc](#)

[Printer-friendly Version](#)

[Interactive Discussion](#)



Malvar, M. C., Prats, S. A., Nunes, J. P., and Keizer, J. J.: Post-fire overland flow generation and inter-rill erosion under simulated rainfall in two eucalypt stands in north-central Portugal, *Environ. Res.*, 111, 222–236, 2011.

5 Malvar, M. C., Martins, M. A., Nunes, J. P., Robichaud, P. R., and Keizer, J. J.: Assessing the role of pre-fire ground preparation operations and soil water repellency in post-fire runoff and inter-rill erosion by repeated rainfall simulation experiments in Portuguese eucalypt plantations, *Catena*, 108, 69–83, 2013.

10 Martins, M. A. S., Machado, A. I., Serpa, D., Prats, S. A., Faria, S. R., Varela, M. E. T., Gonzalez-Pelayo, O., and Keizer, J. J.: Runoff and inter-rill erosion in a Maritime Pine and a eucalypt plantation following wildfire and terracing in north-central Portugal, *J. Hydrol. Hydromech.*, 61, 261–269, 2013.

15 Mayor, A. G., Bautista, S., Llovet, J., and Bellot, J.: Post-fire hydrological and erosional responses of a Mediterranean landscape: seven years of catchment-scale dynamics, *Catena*, 71, 68–75, 2007.

20 Moody, J. A., Shakesby, R. A., Robichaud, P. R., Cannon, S. H., and Martin, D. A.: Current research issues related to post-wildfire runoff and erosion processes, *Earth-Sci. Rev.*, 122, 10–37, 2013.

25 Omar, A. F. B. and MatJafri, M. Z. B.: Turbidimeter design and analysis: a review on optical fiber sensors for the measurement of water turbidity, *Sensing*, 9, 8311–8335, 2009.

30 Postolache, O. A., Silva Girao, P. M. B., Dias Pereira, J. M., and Ramos, H. M.: Multibeam optical system and neural processing for turbidity measurement, *IEEE Sensing Journal*, 7, 677–684, 2007.

35 Prats, S. A., Martins, M. A. S., Malvar, M. C., Ben-Hur, M., and Keizer, J. J.: Polyacrylamide application versus forest residue mulching for reducing post-fire runoff and soil erosion, *Sci. Total Environ.*, 468–469, 464–474, 2014.

40 Prats, S. A., Wagenbrenner, J. W., Martins, M. A. S., Malvar, M. C., and Keizer, J. J.: Hydrological implications of post-fire mulching across two spatial scales, *Land Degrad. Dev.*, under review, 2015.

45 Robichaud, P. R., Elliot, W. J., Pierson, F. B., Hall, D. E., and Moffet, C. A.: Predicting postfire erosion and mitigation effectiveness with a web-based probabilistic erosion model, *Catena*, 71, 229–24, 2007.

## Testing the performance of a turbidity sensor for post-fire runoff

J. J. Keizer et al.

[Title Page](#)

[Abstract](#)

[Introduction](#)

[Conclusions](#)

[References](#)

[Tables](#)

[Figures](#)

◀

▶

◀

▶

[Back](#)

[Close](#)

[Full Screen / Esc](#)

[Printer-friendly Version](#)

[Interactive Discussion](#)



## Testing the performance of a turbidity sensor for post-fire runoff

J. J. Keizer et al.

Title Page

## Introduction

## References

## Figures

1

1

**Close**

Full Screen / Esc

## Interactive Discussion



## Testing the performance of a turbidity sensor for post-fire runoff

J. J. Keizer et al.

**Table 1.** Sediment concentrations and corresponding organic matter contents of the micro-plot scale overland flow samples at the six study sites, and best-fitting power functions between sediment concentration ( $x$ ; in  $\text{g L}^{-1}$ ) with normalized light loss ( $y$ ). Euc. = eucalypt; med = median; iqr = inter-quartile range; 3rd q = third quartile; max = maximum.

site code	parent material	forest type	treatment	no. samples	sediment concentration				om content [%]	best-fitting power function	adjusted $R^2$			
					[ $\text{g L}^{-1}$ ]									
					med	iqr	3rd q	max						
S	schist	euc.	none	112	0.41	0.53	0.72	7.48	61	24	$y = 0.1735x^{0.5983}$	0.64		
			PAM	78	0.64	1.07	1.37	8.19	52	22	$y = 0.1962x^{0.5247}$	0.72		
			mulching	57	0.14	0.20	0.27	2.19	67	21	$y = 0.1268x^{0.6577}$	0.69		
B	schist	euc.	none	33	0.38	0.66	0.85	3.89	54	12	$y = 0.2965x^{0.4938}$	0.77		
D	schist	euc.	none	47	0.21	0.16	0.27	1.06	55	14	$y = 0.2054x^{0.8090}$	0.67		
E	schist	euc.	none	42	0.73	1.76	2.00	6.06	64	29	$y = 0.2510x^{0.5372}$	0.76		
A	granite	euc.	none	19	0.13	0.16	0.22	0.91	58	18	$y = 0.2971x^{0.7912}$	0.81		
C	schist	pine	none	28	0.08	0.12	0.15	1.48	54	12	$y = 0.2808x^{0.6794}$	0.76		

## Testing the performance of a turbidity sensor for post-fire runoff

J. J. Keizer et al.

**Table 2.** Sediment concentrations and corresponding organic matter contents of the slope-scale overland flow samples at the seven study sites, and best-fitting power functions between sediment concentration ( $x$ ; in  $\text{g L}^{-1}$ ) with normalized light loss ( $y$ ). Euc. = eucalypt; med = median; iqr = inter-quartile range; 3rd q = third quartile; max = maximum.

site code	parent material	wildfire	forest type	treatment	no. samples	sediment concentration [ $\text{g L}^{-1}$ ]				om content [%]	best-fitting power function	adjusted $R^2$	
						med	iqr	3rd q	max				
S	schist	burnt	euc.	none	89	0.63	1.07	1.35	8.99	64	16	$y = 0.2272x^{0.6095}$	0.85
					85	0.19	0.41	0.51	1.74	47	23	$y = 0.2163x^{0.7510}$	0.71
B	schist	burnt	euc.	none	45	0.63	0.75	1.09	8.14	58	15	$y = 0.2576x^{0.5670}$	0.89
D	schist	burnt	euc.	none	90	0.29	0.84	1.00	5.86	55	14	$y = 0.1704x^{0.6707}$	0.87
E	schist	burnt	euc.	none	70	1.21	2.26	2.86	8.62	53	12	$y = 0.2768x^{0.5262}$	0.83
A	granite	burnt	euc.	none	73	0.69	1.12	1.39	6.59	38	12	$y = 0.2356x^{0.5944}$	0.86
C	schist	burnt	pine	none	57	0.11	0.32	0.35	6.60	53	19	$y = 0.2281x^{0.6020}$	0.72
F	schist	unburnt	euc.	none	56	0.05	0.14	0.15	0.74	78	22	$y = 0.1314x^{0.5832}$	0.52

Title Page

Abstract

Introduction

Conclusions

References

Tables

Figures

◀

▶

◀

▶

Back

Close

Full Screen / Esc

Printer-friendly Version

Interactive Discussion



## Testing the performance of a turbidity sensor for post-fire runoff

J. J. Keizer et al.

**Table 3.** Sediment concentrations and corresponding organic matter contents of the streamflow samples at the catchment outlet, and best-fitting power function between sediment concentration ( $x$ ; in  $\text{g L}^{-1}$ ) with normalized light loss ( $y$ ). Med = median; iqr = inter-quartile range; 3rd q = third quartile; max = maximum.

no. samples	sediment concentration				om content [%]	best-fitting power function	adjusted $R^2$			
	[ $\text{g L}^{-1}$ ]									
	med	iqr	3rd q	max						
158	0.50	0.83	1.05	4.55	22	8	$y = 0.2809x^{0.7071}$	0.85		

[Title Page](#)

[Abstract](#)

[Introduction](#)

[Conclusions](#)

[References](#)

[Tables](#)

[Figures](#)

◀

▶

◀

▶

[Back](#)

[Close](#)

[Full Screen / Esc](#)

[Printer-friendly Version](#)

[Interactive Discussion](#)



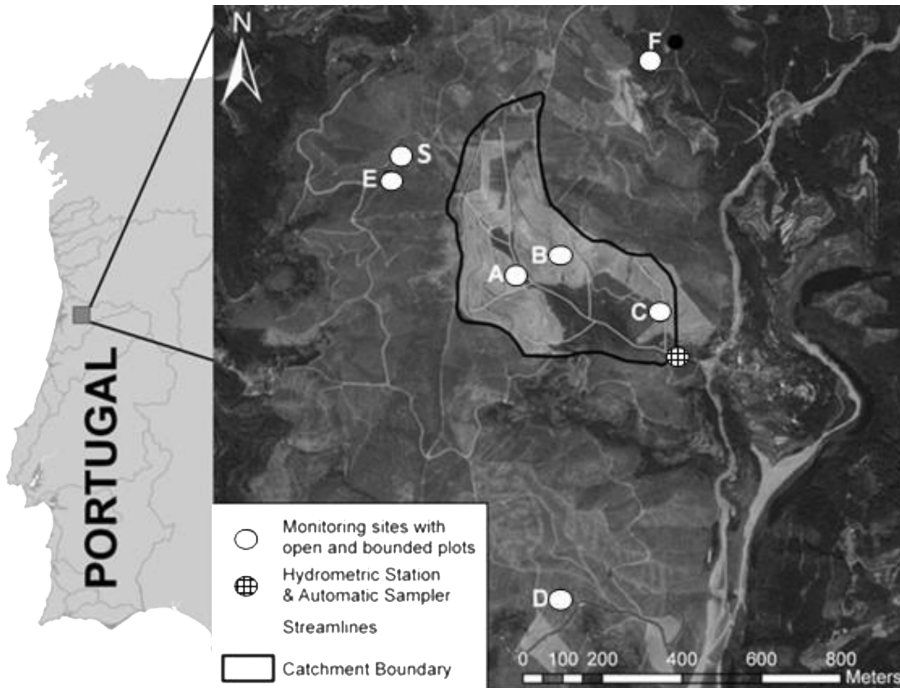


**Figure 1.** Location of the study area, the experimental catchment and the seven study sites (A = burnt eucalypt plantation on granite; B, D, E and S = burnt eucalypt plantations on schist; C = burnt pine plantation on schist; F = long-unburnt eucalypt plantation on schist).

**Testing the performance of a turbidity sensor for post-fire runoff**

J. J. Keizer et al.

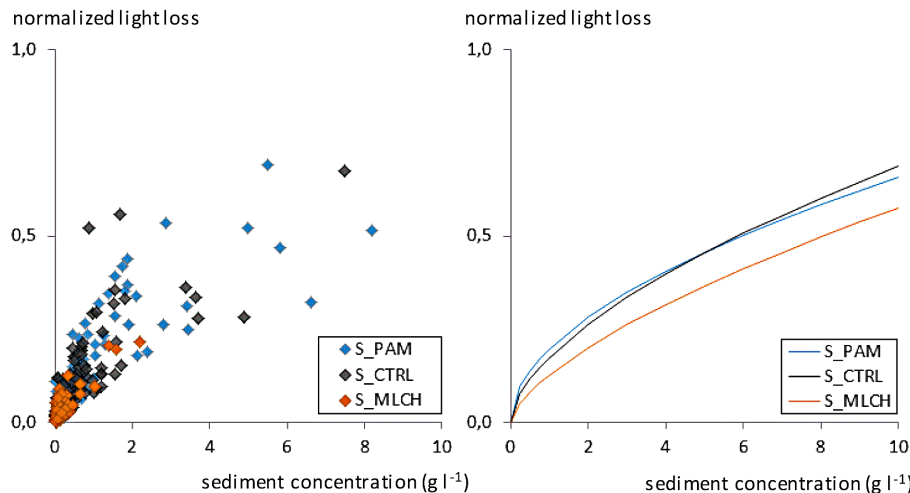


**Figure 2.** Relationships of sediment concentration with normalized light loss at the micro-plot scale for three treatments at study site S (left plot), and corresponding best-fitting power functions (right plot; see Table 1). PAM = polyacrylamide; CTRL = untreated; MLCH = mulching with forest residues.

[Title Page](#)[Abstract](#)[Introduction](#)[Conclusions](#)[References](#)[Tables](#)[Figures](#)[|◀](#)[▶|](#)[◀](#)[▶](#)[Back](#)[Close](#)[Full Screen / Esc](#)[Printer-friendly Version](#)[Interactive Discussion](#)

## Testing the performance of a turbidity sensor for post-fire runoff

J. J. Keizer et al.

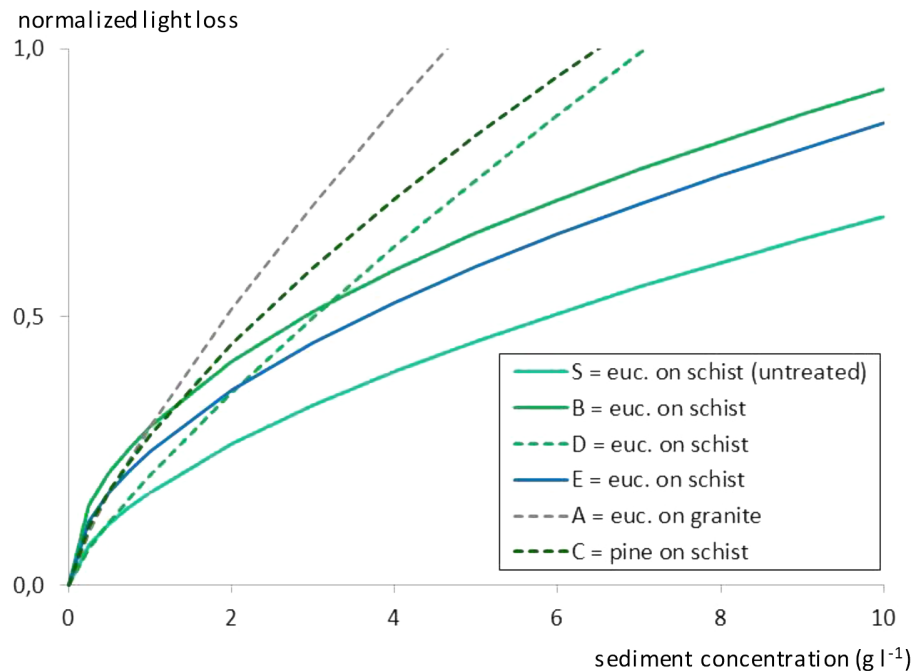


**Figure 3.** Best-fitting power functions of the relationships of sediment concentration with normalized light loss at the micro-plot scale for one pine and five eucalypt plantations (see Table 1).

[Title Page](#)

[Abstract](#)

[Introduction](#)

[Conclusions](#)

[References](#)

[Tables](#)

[Figures](#)

[◀](#)

[▶](#)

[◀](#)

[▶](#)

[Back](#)

[Close](#)

[Full Screen / Esc](#)

[Printer-friendly Version](#)

[Interactive Discussion](#)

**Testing the performance of a turbidity sensor for post-fire runoff**

J. J. Keizer et al.

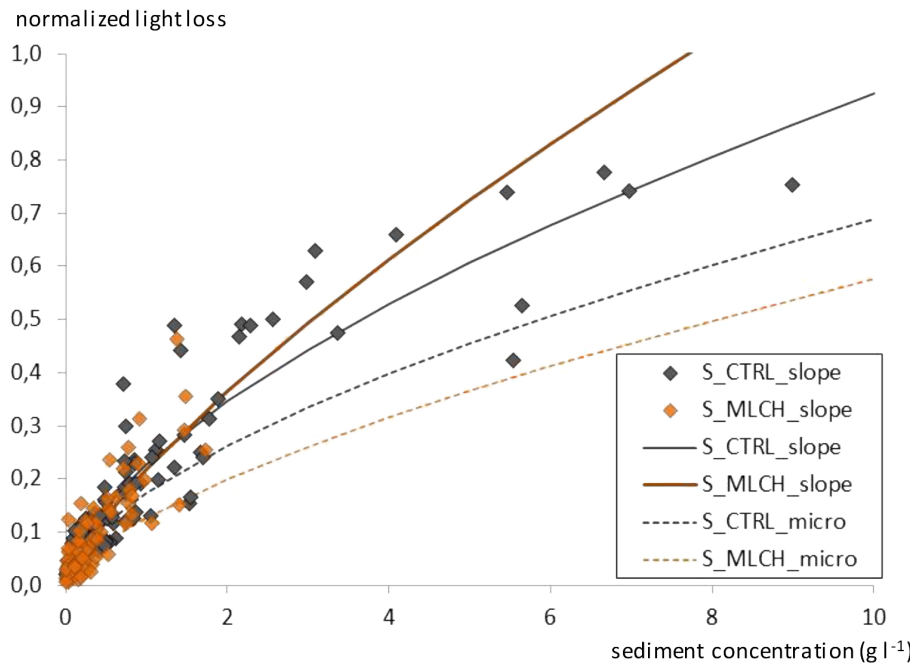


**Figure 4.** Relationships of sediment concentration with normalized light loss at the slope scale for two treatments at study site S, and best-fitting power functions at the slope as well as micro-plot scale (right plot; see Tables 1 and 2). CTRL = untreated; MLCH = mulching with forest residues.

- [Title Page](#)
- [Abstract](#) [Introduction](#)
- [Conclusions](#) [References](#)
- [Tables](#) [Figures](#)
- [◀](#) [▶](#)
- [◀](#) [▶](#)
- [Back](#) [Close](#)
- [Full Screen / Esc](#)
- [Printer-friendly Version](#)
- [Interactive Discussion](#)

**Testing the performance of a turbidity sensor for post-fire runoff**

J. J. Keizer et al.

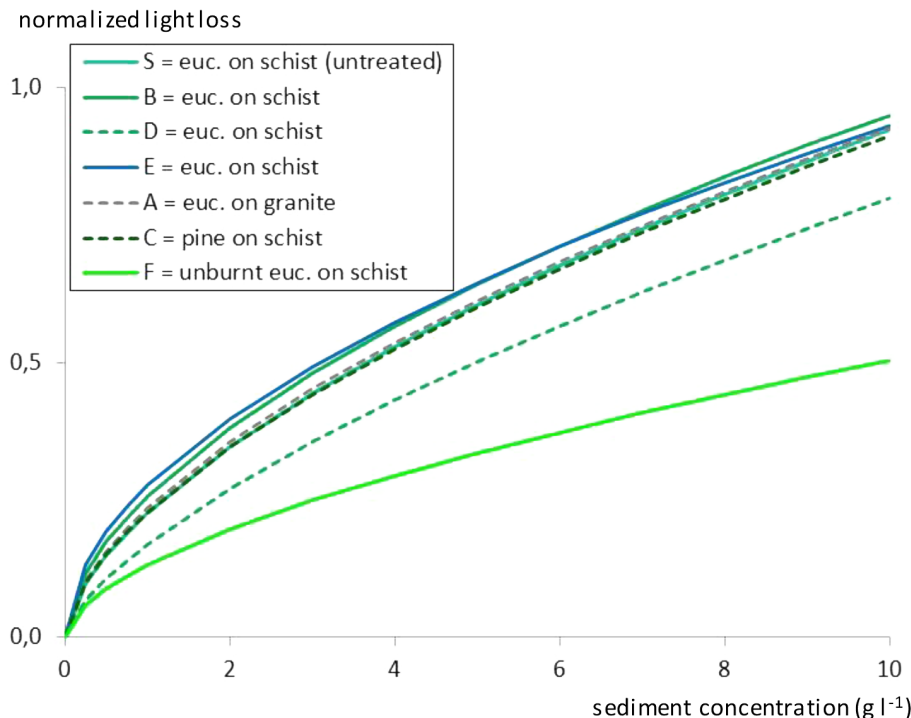


**Figure 5.** Best-fitting power functions of the relationships of sediment concentration with normalized light loss at the slope scale for six recently burnt plantations (one pine and five eucalypt) and one long-unburnt eucalypt plantation (see Table 2).

[Title Page](#)[Abstract](#)[Introduction](#)[Conclusions](#)[References](#)[Tables](#)[Figures](#)[◀](#)[▶](#)[◀](#)[▶](#)[Back](#)[Close](#)[Full Screen / Esc](#)[Printer-friendly Version](#)[Interactive Discussion](#)

**Testing the performance of a turbidity sensor for post-fire runoff**

J. J. Keizer et al.

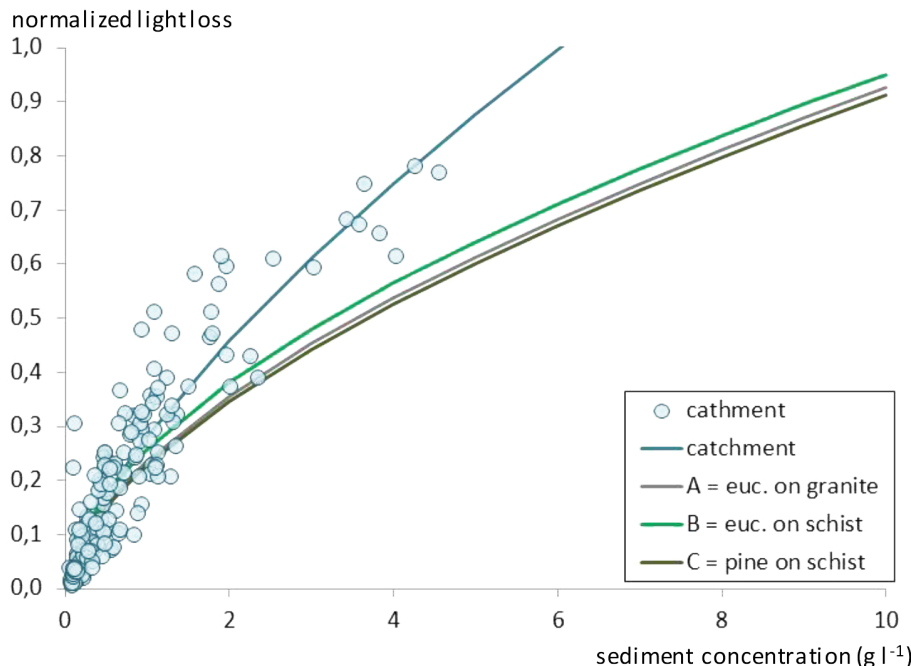


**Figure 6.** Relationships of sediment concentration with normalized light loss at the catchment scale for two treatments, and best-fitting power functions at the catchment as well as slope scale (right plot; see Tables 2 and 3).